Journal of Asian Concrete Federation
Vol. 4, No. 2, pp. 67-78, December 2018
ISSN 2465-7964 / eISSN 2465-7972
https://doi.org/10.18702/acf.2019.1.4.2.67

Technical Paper

Tensile behavior of UHPFRC under uniaxial and biaxial stress conditions

Xiujiang Shen* and Eugen Brühwiler

(Received: March 21, 2018; Accepted: December 14, 2018; Published online: January 04, 2019)

Abstract: Representative and accurate characterization of the tensile behavior of strain hardening Ultra High Performance Fiber Reinforced Cementitious Composite (UHPFRC) remain a challenge. Currently, the uniaxial methods, like direct tensile test (DTT) and 4-point bending test (4PBT), are commonly applied, although the biaxial tensile condition has been widely recognized in the UHPFRC applications, e.g. thin UHPFRC layers as external reinforcement for RC slabs. In this paper, results from ring-on-ring testing of circular slab-like specimens are presented to determine the equi-biaxial tensile response by means of inverse analysis using 3D finite element method (FEM). In addition, DTT, using structural specimens cut from large square plates, and 4PBT, using standard specimens cast in mould individually, were carried out. The tensile response from 4PBT was derived through inverse analysis using 2D FEM. Finally, the corresponding results from the three different testing methods under either uniaxial or biaxial stress condition were analyzed and compared in terms of tensile characteristic parameters, tensile material law, fracture process, and energy absorption capacity. While the three testing methods did not show significant difference in tensile strength, significantly higher strain hardening deformation was identified in the case of biaxial stress conditions.

Keywords: biaxial stress condition, FEM, inverse analysis, ring-on-ring test, UHPFRC, uniaxial stress condition, tensile behavior.

1. Introduction

The tensile response is a fundamental constitutive property of strain hardening Ultra High Performance Fiber Reinforced Cementitious Composite (UHPFRC), so the accurate and representative characterization of this response is necessary for the design of a given UHPFRC application. In general, this characterization is achieved by means of uniaxial test methods, especially direct tensile test (DTT) and 4-point bending test (4PBT) using small-scale laboratory specimens casting in moulds individually. Unfortunately, these tests exhibit considerable scatter and the results are often considered as an upper bound in case of small-scale laboratory specimens, hardly reproducing real design situations. Most infrastructures, in particular bridge decks and floors, are principally under biaxial stress condition, far from uniaxial stress state [1]. In this context, the actual tensile performance of UHPFRC under biaxial stress condition should be investigated and compared with that from uniaxial stress condition carefully.

The DTT using dumbbell-shaped specimen is commonly applied to determine directly the uniaxial tensile properties of UHPFRC for given preparation conditions (moulds, casting, and curing). For reliable results, wise design and preparation are required when conducting DTT. In order to avoid largely the initial eccentricity with bending effects, the specimen was built-in the testing machine by applying the principle "gluing without adherence", developed by Helbling & Brühwiler [2]. This method was also applied in ref. [3,4]. Proposed by Graybeal et al. [5,6], the tapered aluminum plates were fixed to both sides of each specimen end to ensure final fracture occurs out of the central constant part. Otherwise, one or two layers of steel wire mesh were used to strengthen each end of specimen, as applied in ref. [7,8]. Additionally, boundary conditions also have important influence on test results, and the fixed conditions is

Corresponding author Xiujiang Shen is a doctoral candidate, Maintenance and Safety of Structures (MCS-ENAC), Ecole Polytechnique Fédérale de Lausanne (EPFL), GC B2-402, Station 18, CH-1015 Lausanne, Switzerland (Email: xiujiang.shen@epfl.ch).
Eugen Brühwiler is a professor, director of Maintenance and Safety of Structures (MCS-ENAC), Ecole Polytechnique Fédérale de Lau-sanne (EPFL), GC B2-402, Station 18, CH-1015 Lau-sanne, Switzerland
(Email: eugen.bruehwiler@epfl.ch).

recommend for reliable estimation of tensile response of UHPFRC after elastic limit, as confirmed by Kanakubo [9]. The 4PBT, alternatively, was used successfully to identify the tensile property of UHPFRC indirectly by means of inverse analysis, including analytical method and FEM [10–12].

Regarding direct biaxial tests, four actuators and a big frame are generally necessary, and inherently, many challenges pertaining to uniform load distribution, frictional effect, accurate boundary condition and load control need to be addressed carefully. Therefore, only few studies have been conducted on the biaxial behavior of concrete [13,14], especially no experimental study on biaxial behavior of UHPFRC has been recorded through direct biaxial test. Recently, the ring-on-ring test, as a 3D version of 4PBT, has been developed to investigate the biaxial flexural strength of concrete [15–17]. This method was extended to UHPFRC by several researchers [1]. The limited test results show that the ring-on-ring test allowed the actual development of fiber bridging effects between cracks, thus accurately representing the behavior of UHPFRC members subjected to biaxial flexural loading.

In this paper, the ring-on-ring test on circular slab-like specimens has been developed to determine the equi-biaxial tensile response. In addition, direct tensile tests using dumbbell specimens cut from large square plates and 4PBT using small plates cast in molds were carried out. The corresponding tensile response from five DTT, six 4PBT and four ring-on-ring tests were analyzed and compared (See Fig. 1). The main objective was to examine the differences and relationships of the tensile response of UHPFRC under uniaxial and biaxial stress conditions, and to propose the most appropriate test method to determine the tensile property for a given UHPFRC application.

2. Experimental Program

2.1 Ring-on-ring test

The ring-on-ring test method was applied for indirect characterization of the tensile behavior under biaxial stress condition, using circular slab-like specimens with a diameter R = 600 mm and a thickness h = 50 mm. This method has been extensively adopted and even standardized by ASTM [18] in the ceramics and glass domain. Recently, this method was modified and validated to measure the biaxial flexural strength of concrete and UHPFRC [15–17,19,20]. The updated ring-on-ring test yielded stable test results with small scatter, and it is promising to be a reliable and rational means to investigate biaxial flexural behavior of UHPFRC.

Figure 2 shows the full test set-up and devices applied in this experimental campaign. The slab was simply supported on a steel support ring with R = 500 mm. Loading was imposed by a hydraulic jack acting on the center of slab through a steel force transmitting ring with r = 150 mm. All the slabs were subjected to three loading–unloading cycles to 20 kN with an actuator displacement rate of 1.0 mm/min. Afterwards, monotonic loading with the same displacement rate was applied up to the peak force, followed by a rate of 4.0 mm/min until the actuator displacement reached 80 mm. Under loading, the uniform stress is introduced on the bottom surface within the force transmitting ring area, where biaxial stress condition is assumed.

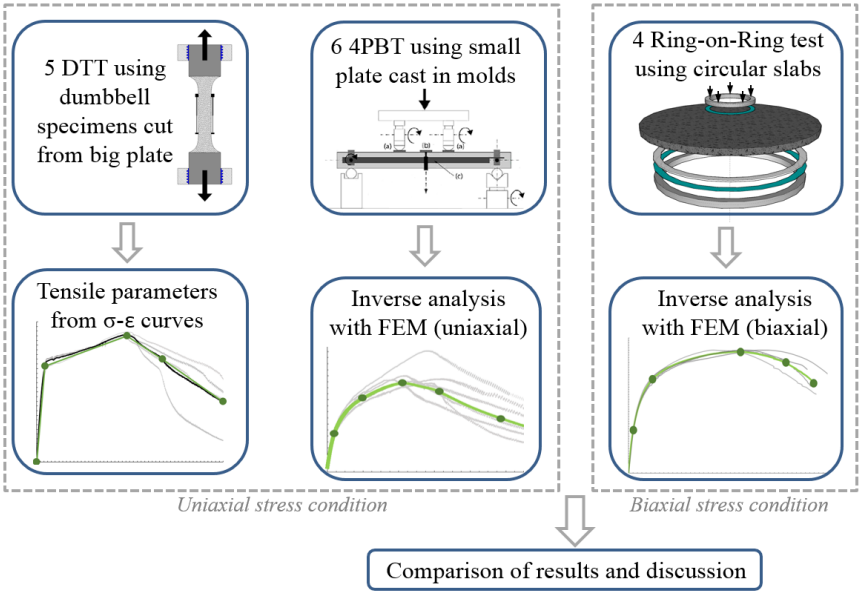

Fig. 1 – Approach for the comparison of the tensile response of UHPFRC under uniaxial and biaxial stress conditions

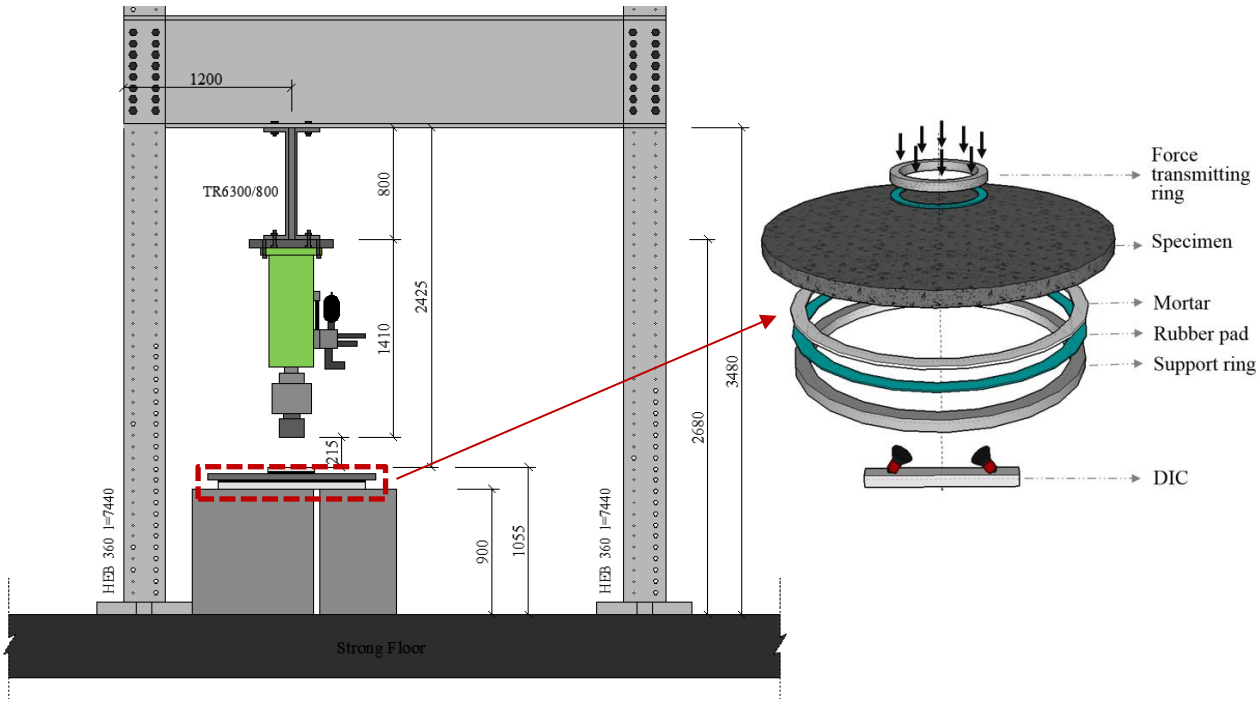

Fig. 2 – Schematic description of test setup (unit: mm)

The slabs were tested with the casting surface facing upwards, allowing the observation of tensile crack propagation on the smooth sheathed surface. Before testing, the casting surface was polished and a mortar layer was placed between support ring and bottom surface to level out both surfaces. Two rubber pads (thickness of 10 mm, E = 500 MPa) were positioned between the slab surfaces and the two rings to distribute the force evenly.

As illustrated in Fig. 2, Digital Image Correlation (DIC) technique was applied to observe the deflection development, strain field, and micro-cracking during the whole testing process. Two digital cameras were placed underneath the slab at a distance of 0.5 m and an angle of 23 degrees to the vertical. The tensile surface of the slab was painted with matte white paint, and then spayed black speckle pattern with size less than 1 mm. The targeted area, which was visible to the DIC, was about Ø500 mm on the center of the slab. In such case, the DIC measurement accuracy can reach around 5 με. In addition, several LVDTs were installed on the top surface to measure the deflection. All deflection measurements were performed with respect to the strong floor. The measurement frequency was 5 Hz. Further details about the ring-on-ring test applied in this study can be found in [21].

2.2 Direct tensile test (DTT)

The dumbbell shaped specimens, with a constant cross section of 80 mm × 50 mm at the central part, were adopted for uniaxial DTT. The geometry of specimen was designed based on the equation of Neuber's spline [22,23]. In total five specimens were extracted from a large square plate (1,100 mm × 1,100 mm × 50 mm) with the same thickness and casting procedure as that for the circular slab-like specimen (See Fig. 3). This allowed to assess the variability of tensile behavior in the plate.

The tensile tests for all specimens were performed on a universal servo-hydraulic testing machine with a capacity of 1,000 kN, according to SIA 2052 [24]. The Digital Image Correlation (DIC) technique and three different series of sensors were adopted to measure the deformation and crack opening of the UHPFRC, as shown in Fig. 4. Further details about the developed DTT in this study can be found in ref. [3].

2.3 Four-point bending test (4PBT)

In total six small plate specimens with dimension of 500 mm × 100 mm × 3 mm were cast individually in molds. The 4PBT for all specimens was performed on a universal servo-hydraulic testing machine with a capacity of 200 kN, according to SIA 2052 [10,24]. The total span of the four-point bending test set up was 420 mm (See Fig. 5), and the supports allowed free displacement of the specimen along its longitudinal axis. Two transducers placed on a measuring frame on each side of the specimen measured the net deflection in the center of the span. The measurements were taken at a frequency of 5Hz during the test.

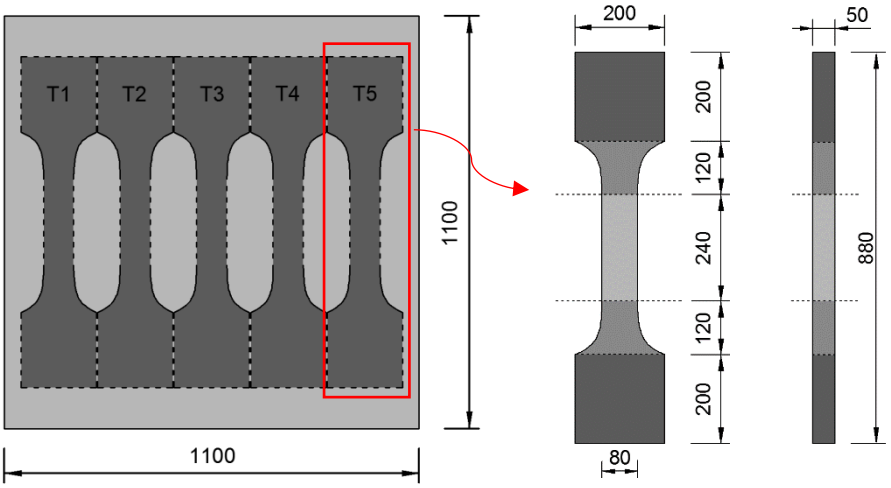

Fig. 3 – Extracting of dumbbell specimens and dimension of dumbbell specimen (unit: mm)

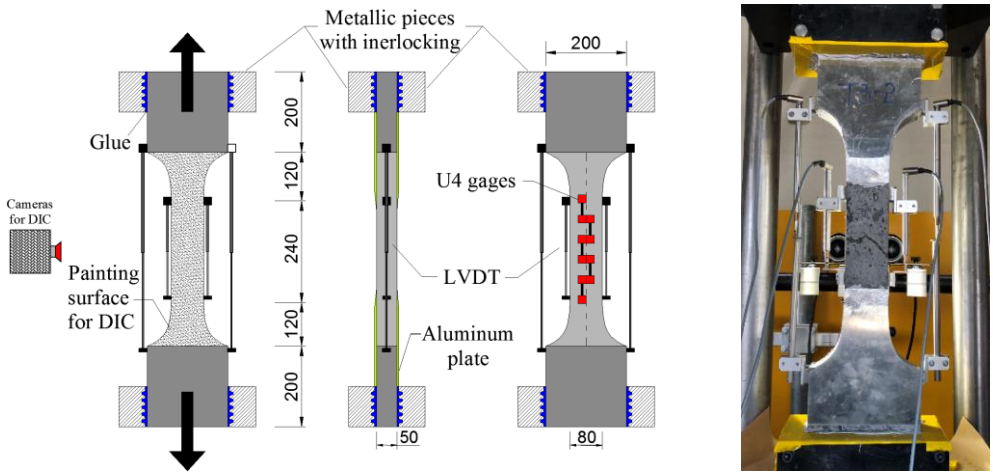

Fig. 4 – Tensile test setup and instrumentation for the dumbbell specimens (unit: mm)

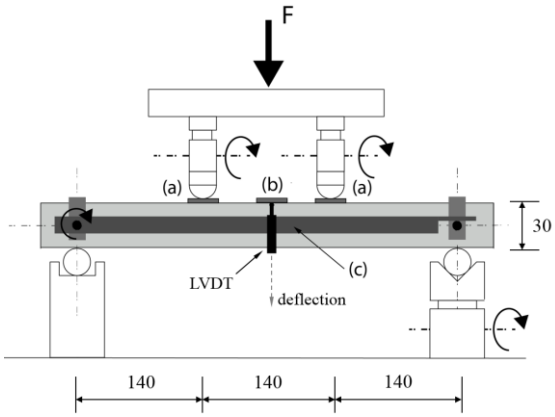

(a) two application points of t he displacements;
(b) reference wafer fixed on th e upper specimen surface;
(c) metallic frame placed at m id-height of the specimen

Fig. 5 – Four-point bending test setup and instrumentation (unit: mm) [24]

2.4 Fabrication and curing

The chosen UHPFRC is an industrial premix containing 3.8% by volume of straight steel fibers with length of 13 mm and diameter of 0.175 mm, and its water/cement ratio is 0.15. The UHPFRC was mixed to obtain a batch of 180 liters. The large square plate and circular slab-like specimens were cast in one step: the fresh UHPFRC mixture was

poured in the center of the formworks, and let flow without any pulling or vibration. Regarding the small plate specimens for 4PBT, the fresh mixture was poured from one side and let flow. Once the casting was completed, a plastic sheet was pulled over the specimens to allow for auto-curing of the material. The specimens were demolded after 24 hours, then kept under moist curing conditions (20℃, 100% humility) for the following seven days; and subsequently, stored inside the laboratory until testing. The test age was more than 60 days, given that more than 90% of the UHPFRC material properties is attained after 60 days [4,25].

3. Test Results

3.1 Uniaxial tensile response from DTT

In Figure 6, the DTT results of five specimens are presented in terms of stress-strain (σ-ε) curves, in which the thick black line represents the average response. The stress is defined as the measured force divided by the constant cross-sectional area of dumbbell specimen, while the strain is based on the average value measured from two short LVDTs with measuring length of 160 mm. The main characteristic tensile parameters for each specimen are summarized in Table 1, including elastic modulus E_U, elastic limit point (stress f_{Ute} and corresponding strain ε_{Ute}), and ultimate point (f_{Utu} and ε_{Utu}). Here, the end of the linear relationship in σ-ε curve is regarded as elastic limit point, and the beginning of the tensile softening response is defined as ultimate point. The average curve is obtained through averaging 5 normalized curves, where the stress and strain are divided by the corresponding values at peak point (f_{Utu} and ε_{Utu}), respectively. As shown in Fig. 6 and Table 1, a considerable variation of tensile response, strain-hardening behavior in particular, is observed. This is attributed to the variability of fiber distribution in different specimens depending on the distance from the pouring point [3]. In this case, due to the high fluidity and workability of the UHPFRC material, the fresh mixture flowed freely from the center to the border in radial direction. The flow exerted forces on the fibers, pushing fibers to align more perpendicularly to the flow direction, as illustrated in Fig. 7. Additionally, based on a previous study [3], random fiber distribution and orientation can be assumed for specimen T2~T4 around the pouring point.

Based on DIC analysis using VIC-3D, the whole microcracking and fracture process of each specimen is captured effectively during the loading process. The initiation and propagation of fine micro-cracks in the strain-hardening domain, in particular, can be detected visually in DIC full-field strain maps. The representative fracture process shown by T3 is illustrated in Fig. 8. Generally, point A (elastic limit) refers to the start of strain-hardening response in UHPFRC, symbolized by the activation of first fine micro-cracks; while point B (ultimate limit) stands for the end of this response, characterized by the formation of one single localized fictitious crack by grouping of several fine micro-cracks. Afterwards (beyond point B), the fictitious crack shows significant stress transfer through the fibers bridging the two crack sides and develops with increasing crack opening until no more stress is transferred when a crack opening of half the fiber length is reached, i.e., in present case, 6.5 mm (= $Lf/2$). It is important to note that the microcracks are mostly concentrated in two local zones with random distribution of several micro-cracks over a large extent (> Lf).

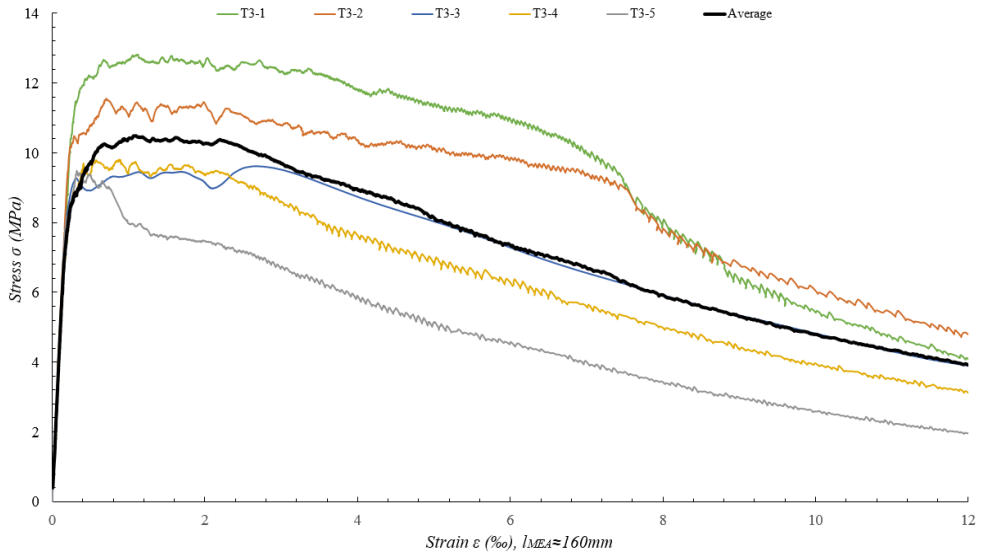

Fig. 6 – Tensile response from DTT

Table 1 – Tensile parameters from DTT

N°	E_U [GPa]	*fUte* [MPa]	*fUtu* [MPa]	*fUtu/fUte*	*εUte* [‰]	*εUtu* [‰]
T1	45.60	9.70	12.23	1.26	0.22	3.48
T2	49.09	9.41	11.21	1.19	0.20	2.33
T3	47.39	7.74	9.62	1.24	0.17	2.68
T4	49.64	7.25	9.48	1.31	0.17	2.15
T5	48.38	7.20	9.10	1.26	0.16	0.68
Average	48.02	8.26	10.33	1.25	0.18	2.26
Std. dev.	1.59	1.21	1.33	0.04	0.03	1.02
COV	0.03	0.15	0.13	0.03	0.14	0.45

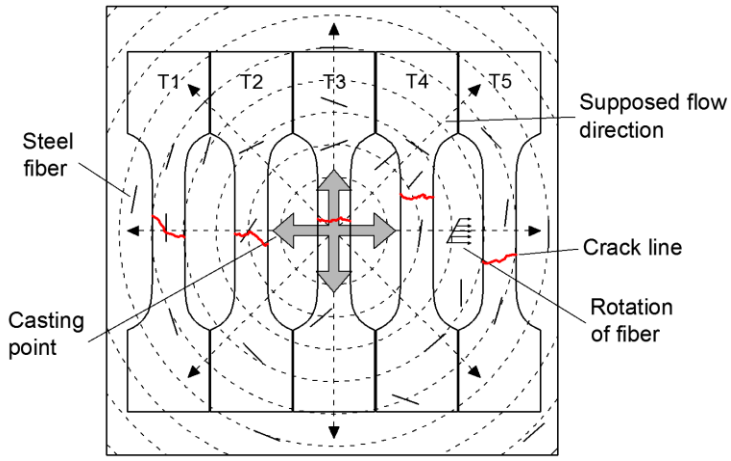

Fig. 7 – Final crack positions of dumbbell specimens and schematic view of fiber distribution in the plate

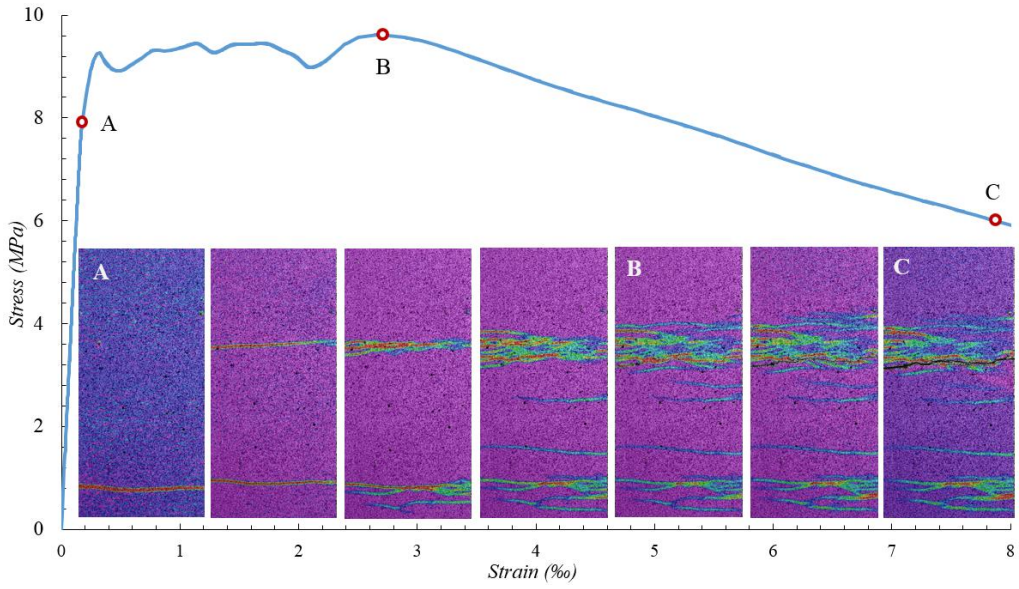

Fig. 8 – Representative microcracking and fracture process of UHPFRC specimen under DTT

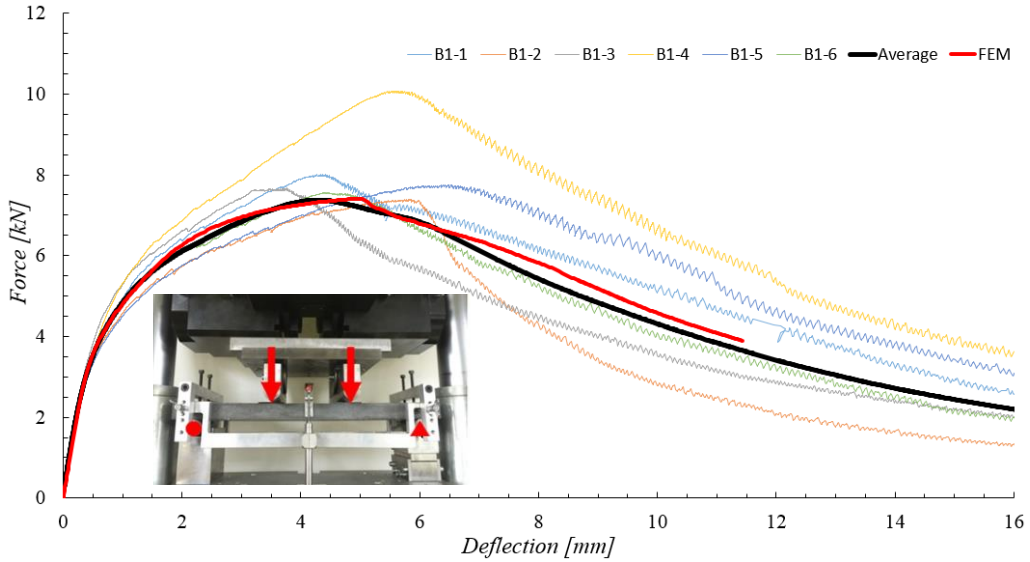

Fig. 9 – Bending response from 4PBT

3.2 Uniaxial tensile response based on inverse analysis from 4PBT

Figure 9 presents the bending behavior from 4PBT in terms of force-deflection curves, in which the thick black curve is the average response. All curves agree well with each other, showing comparable bending behaviour. This results from the similar fiber distribution and orientation in the small plate specimens, given that they were fabricated individually in moulds following the same casting procedure.

The uniaxial tensile response of UHPFRC is evaluated indirectly by means of inverse analysis of 4PBT results using non-linear Finite Element Analysis (FEA). A 2D FE model was built using the non-linear FE analysis software DIANA (smeared crack model), targeting at simulating the bending behaviour in terms of force-deflection response and cracking pattern of small plate specimens under 4PBT. The best results of FE model fitting with the average experimental curve is shown in Fig. 9, where a close fit is achieved, as indicated by the thick red curve. The corresponding uniaxial tensile parameters are summarized in Fig. 13 and Table 2.

3.3 Biaxial tensile response based on inverse analysis from ring-on-ring test

The biaxial flexural responses of four UHPFRC circular slabs from ring-on-ring tests are presented in terms of force-deflection curve (F - δ) of the center point, as shown in Fig. 10**.** The recorded force value was adjusted considering a geometry factor that accounts for the precise thickness of each slab. The deflection was measured by DIC on the bottom surface, excluding the deformation of the rubber pad measured from three LVDTs on the top surface. It is obvious that all slabs show a consistent flexural response with little scatter. Up to a force value of about 40kN, the flexural behavior of the UHPFRC slabs in terms of F-δ curve is almost linear, and the end of this linearity is herein defined as elastic limit (point A). Afterwards, a quasi-linear response (II, A-B) with a slight decrease of stiffness is noticed, in which the formation and propagation of multiple microcracks are expected. And sequentially, significant deflection hardening behaviour is identified until the peak point (C) is reached. Afterwards, the slabs exhibit important ductility with high residual resistance in the softening phase (IV C-D). Further details about the test results are described in [21].

Furthermore, the representative microcracking and fracture process from S1-3, as observed by DIC on the visualized central portion (400 mm × 400 mm), is shown in Fig. 11. The selected DIC images in Fig. 11 represent the crack patterns in different characteristic phases following the F-δ curve, and the white dash circle marks the position of the force transmitting ring.

Accordingly, several phenomena characterizing microcracking process of UHPFRC slabs are identified. Once the elastic limit (A) is reached, the first microcracks with random distribution initiate within the force transmitting ring area, where the tensile stress is uniform and maximal in all directions. Afterwards, these microcracks start to propagate irregularly, and more new microcracks are generated until point B is reached. In this phase II, the microcrack pattern changes continuously with increasing deflection and has a complex distribution, microcracks initiate randomly with irregular propagation paths; some of them produce multiple branches, and some

cross each other or combine together during propagation. At point B, several fine fictitious cracks ($w \geq$ 0.05 mm) are detected by DIC, and afterwards, more microcracking appears with increasing deflection. Fine fictitious cracks initiate from some of previous microcracks in phase II, and largely concentrate within the force transmitting ring area. Some fine fictitious cracks are localized at peak force (point C), and then propagate radially from the center to the edge with increasing crack opening in the softening phase (C-D). No additional cracks form beyond point C.

Similarly, in order to determine the biaxial tensile response of UHPFRC, the inverse analysis of the ring-on-ring test results was conducted by means of a 3D FE analysis using DIANA software. Considering the random fiber distribution in the slab, the full scale of the slab element was modeled, and the smeared crack concept was adopted. The boundary conditions in simulation of ring-on-ring test have a strong influence on the stability of the numerical procedure and on the fracture pattern. During testing, the specimens were not prevented from sliding and lifting from the supporting ring along fracture growth. Therefore, the two adjacent ¼ points of the support ring were only constrained in tangential directions, and the top surface central point was constrained in both X and Y directions. Additionally, the interface elements were built between the specimen and the rubber pads, avoiding tensile reaction force from the supporting ring. The base and verification of FE model are described in ref. [21]. The modeling results with best fitting of F-δ curve with respect to the average response is illustrated in Fig. 10 (red line), where a close fit is achieved. The results from the inverse analysis are summarized in Fig. 13 and Table 2.

4. Discussion

Finally, all the tensile responses under uniaxial or biaxial stress condition based on different methods, are summarized in Fig. 13 and Table 2. Regarding DTT, the average response from specimen T2~T4 is used for further comparison, since their locations in the large plate correspond to the area under biaxial stress condition in ring-on-ring test. The uniaxial tensile response from 4PBT cannot be applied directly, due to favorable fiber alignment in the small plates along the loading direction. This phenomenon is attributed to the small geometry of the mould and specific casting process as described in section 2.4. Thus, fiber distribution and orientation effect should be considered for better comparison.

Based on a previous study on an UHPFRC layer with thickness of 50 mm [12], the average fiber orientation factor (μ_0) was identified in the range of 0.53~0.60. In this study, the mean value is applied, namely $\mu_0 = 0.57$, for the DTT specimens, given that random fiber distribution may be assumed in the central part of the large plate. For a UHPFRC layer or small specimen with thickness of 30 mm, μ_0 was determined in the range of 0.61~0.70 in ref. [12]. Thus, the upper limit ($\mu_0 = 0.70$) is chosen for 4PBT specimens, respecting preferential fiber alignment in small plates. The corresponding efficiency factor (μ_1) is obtained for both cases (0.94 and 0.96, respectively) based on Fig. 10. Accordingly, the uniaxial tensile response from 4PBT is modified to be representative for the large plate in the case of random fiber distribution, the results are also summarized in Fig. 13 and Table 2.

As observed in Fig. 13 and Table 2, in general, the tensile performance in terms of strength from both uniaxial and biaxial stress states are quantitatively similar. This phenomenon can be attributed to the fact that all the test methods provide the specimens with a certain area of uniform stress, allowing for initiation of microcracks and localization of fictitious cracks at local weaker zones with respect to the main stress direction. Thus, the tensile performance largely depends on the distribution and size of local weaker zones. In the case of random fiber distribution, the local weaker zones can be assumed to distribute randomly without any considerable preference in all directions.

Additionally, it should be noted that a significant increase in hardening strain ε_{Utu} is found under biaxial stress state. This effect can be due to the fact that many more fibers in different directions contributed to the bridging and debonding effects under biaxial stress state, offering considerably higher ductility and toughness including larger deformation, compared with the results from specimens with uniaxial stress state, where fibers perpendicular to the loading direction have no contribution. This difference can also be explained by the different cracking patterns under different stress states, as illustrated in Figs. 8 and 11. The circular slab subjected to biaxial stress state shows a large amount of microcracks distributed densely and randomly on the tensile surface in strain-hardening domain (phase II, AB), and most microcracks developed along irregular paths are interlocked. Sequentially, several fictitious cracks appeared. In the case of the DTT specimens under uniaxial stress state, the microcracks concentrated locally at weaker zones and propagated from one edge to the other following a relatively linear path, and only one or two fictitious cracks localized finally.

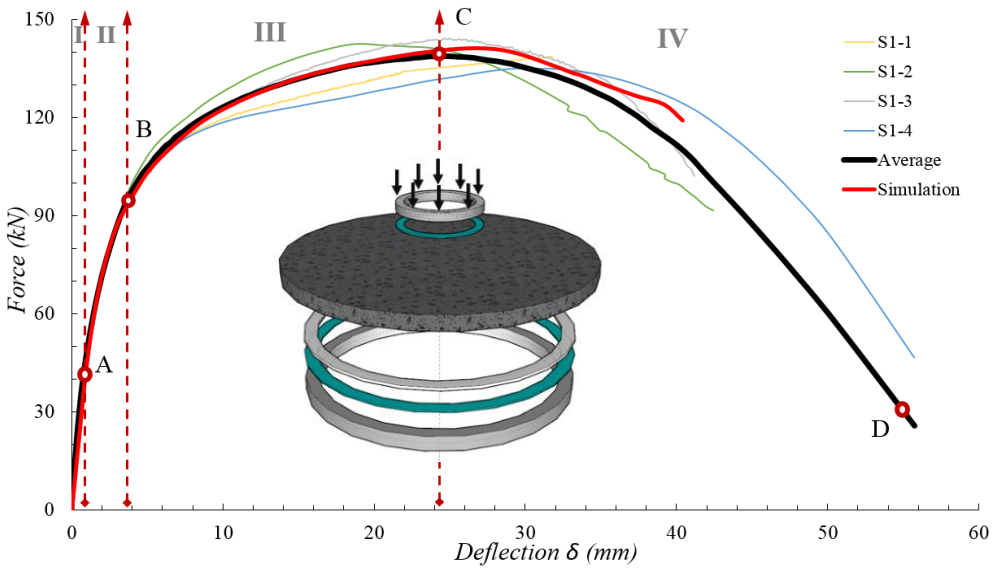

Fig. 10 – Biaxial flexural response from the ring-on-ring tests

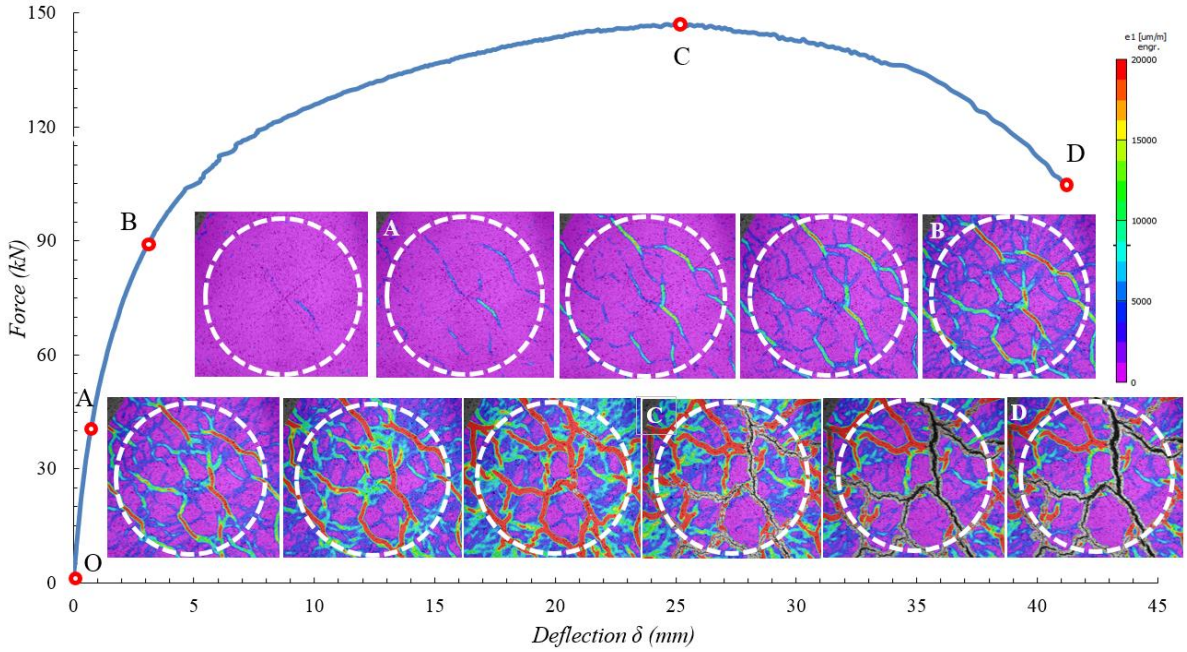

Fig. 11 – Representative microcracking and fracture process of UHPFRC slab of a ring-on-ring test specimen.

Table 2 – Tensile parameters from the three different test methods

Test Method	E_U [GPa]	f_{Ute} [MPa]	f_{Utu} [MPa]	f_{Utu}/f_{Ute}	ε_{Ute} [‰]	ε_{Utu} [‰]
DTT	49	8.13	10.10	1.24	0.18	2.39
4PBT	51	10.00	14.00	1.40	0.20	3.92
4PBT (modified)	51	8.00	11.20	1.40	0.16	3.14
Ring-on-ring test	50	9.60	11.35	1.18	0.19	5.54

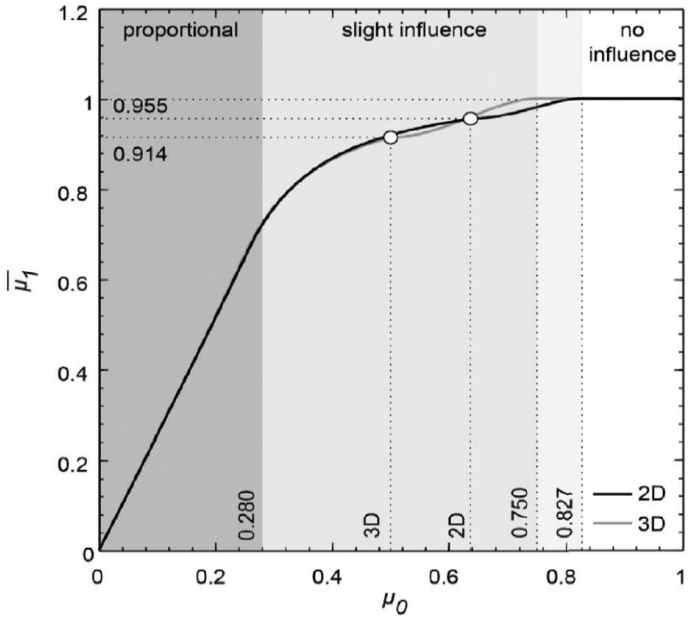

Fig. 12 – Relationship between orientation factor μ_0 and efficiency factor μ_1 [12]

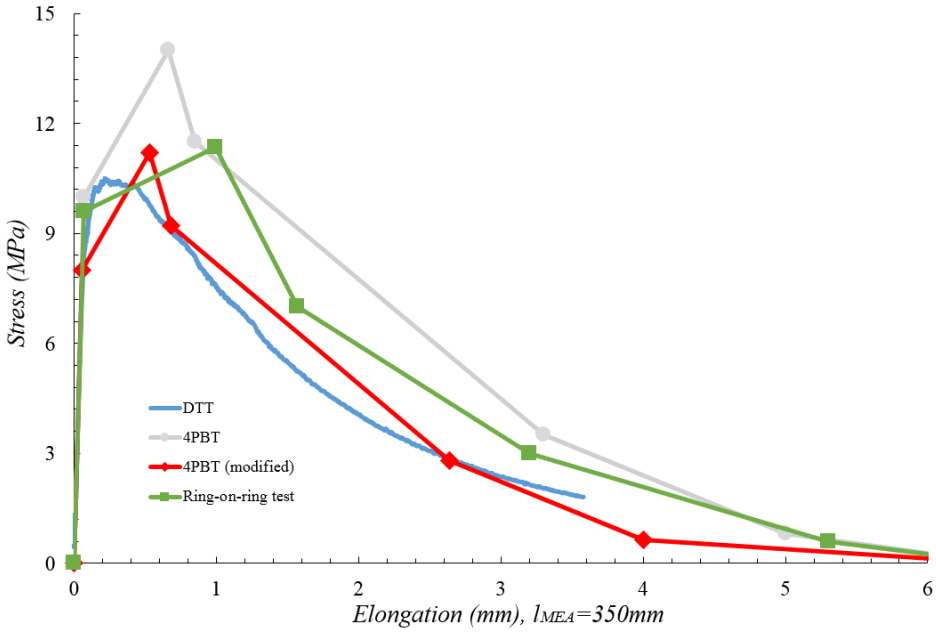

Fig. 13 – Tensile responses from the three different test methods

5. Conclusions

This study investigated the tensile behavior of UHPFRC under uniaxial and biaxial stress conditions by means of DTT, inverse analysis based on 4PBT, and ring-on-ring test results using FEM. The results suggest that the tensile response of UHPFRC is not an intrinsic property and depends on several factors, including the specimen geometry, flow regime of fresh mixture during casting, and the stress condition imposed on the specimen.

In the case of random fiber distribution, there is no significant difference of tensile performance in terms of strength between uniaxial and biaxial stress conditions. Furthermore, since more fibers are activated, the multiple microcracking behavior is more

pronounced and complex under biaxial stress condition, resulting in a significantly higher strain hardening deformation ε_{Utu}, compared with uniaxial stress condition. Consequently, when the fibers are distributed randomly, it is conservative to use uniaxial tensile parameters as obtained from DTT or 4PBT, to design UHPFRC structural elements or UHPFRC strengthening layers on concrete substrates subjected to biaxial stress condition.

References

1. J. Kim; D.J. Kim; S.H. Park; and G. Zi (2015) "Investigating the flexural resistance of fiber reinforced cementitious composites under biaxial condition," Composite Structures, 122, pp. 198–208.
2. A. Helbling and E. Brühwiler (1987) "Eine neue Halterung für Zugversuche mit Beton-Probekörper," Material Und Technik, 4, pp. 103–107 (*in German*).
3. X. Shen and E. Brühwiler "Characterization of Tensile Beahvior in UHPFRC Thin Slab Using NDT Method and DIC System," Proceedings PRO 129, Fuzhou, China, November 2018.
4. K. Habel (2004) Structural behaviour of elements combining ultra-high performance fibre reinforced concretes (UHPFRC) and reinforced concrete, Doctoral Thesis, EPFL, Swizterland.
5. B.A. Graybeal and F. Baby (2013) "Development of Direct Tension Test Method for Ultra-High-Performance Fiber-Reinforced Concrete," ACI Materials Journal, 110(2), pp. 177-186.
6. A. Abrishambaf; M. Pimentel; and S. Nunes (2017) "Influence of fibre orientation on the tensile behaviour of ultra-high performance fibre reinforced cementitious composites," Cement and Concrete Research, 97, pp. 28–40.
7. S. Gwon and M. Shin (2016) "Direct-tensile and flexural strength and toughness of high-strength fiber-reinforced cement composites with different steel fibers," Journal of Asian Concrete Federation, 2(1), pp. 67–80.
8. M. Shin; S.-W. Gwon; K. Lee; S.W. Han; and Y.W. Jo (2014) "Effectiveness of high performance fiber-reinforced cement composites in slender coupling beams," Construction and Building Materials, 68, pp. 476–490.
9. T. Kanakubo (2006) "Tensile Characteristics Evaluation Method for Ductile Fiber-Reinforced Cementitious Composites," ACT, 4, pp. 3–17.
10. E. Denarié; L. Sofia; and E. Brühwiler (2017) "Characterization of the tensile response of strain hardening UHPFRC - Chillon Viaducts," AFGC-ACI-Fib-RILEM Int. Symposium on Ultra-High Performance Fibre-Reinforced Concrete, UHPFRC 2017.
11. SAMARIS D26 (2006) Modelling of UHPFRC in composite structures, European project 5th FWP / SAMARIS – Sustainable and Advanced Materials for Road Infrastructures – WP 14: HPFRCC (http://samaris.zag.si/).
12. M. Bastien-Masse; E. Denarié; and E. Brühwiler (2016) "Effect of fiber orientation on the in-plane tensile response of UHPFRC reinforcement layers," Cement and Concrete Composites, 67, pp. 111–125.
13. S.-K. Lee; Y.-C. Song; and S.-H. Han (2004) "Biaxial behavior of plain concrete of nuclear containment building," Nuclear Engineering and Design, 227, pp. 143–153.
14. W. Swanepoel (2011) The behaviour of fibre reinforced concrete (SHCC) under biaxial compression and tension, Stellenbosch: Stellenbosch University.
15. G. Zi; H. Oh; and S.-K. Park (2008) "A novel indirect tensile test method to measure the biaxial tensile strength of concretes and other quasibrittle materials," Cement and Concrete Research, 38, pp. 751–756.
16. O. Ekincioglu (2010) A discussion of paper "A novel indirect tensile test method to measure the biaxial tensile strength of concretes and other quasibrittle materials" by G. Zi, H. Oh, S.K. Park, Cement and Concrete Research, 40, pp. 1769–1770.
17. J. Kim; D.J. Kim; and G. Zi (2013) "Improvement of the biaxial flexure test method for concrete," Cement and Concrete Composites, 37, pp. 154–160.
18. ASTM C1499-05 (2009) Standard test method for monotonic equibiaxial flexural strength of advanced ceramics at ambient temperature, ASTM International, West Conshohocken, Pennsylvania.
19. D.-Y. Yoo; G. Zi; S.-T. Kang; and Y.-S. Yoon (2015) "Biaxial flexural behavior of ultra-high-performance fiber-reinforced concrete with different fiber lengths and placement methods," Cement and Concrete Composites, 63, pp. 51–66.
20. D.-Y. Yoo; N. Banthia; G. Zi; and Y.-S. Yoon (2017) "Comparative Biaxial Flexural Behavior of Ultra-High-Performance Fiber-Reinforced Concrete Panels Using Two Different Test and Placement Methods," Journal of Testing and Evaluation, 45(2), pp.624-641
21. X. Shen and E. Bruehwiler (2017) "Flexural quasi-static behavior of UHPFRC circular slab specimens," AFGC-ACI-Fib-RILEM Int. Symposium on Ultra-High Performance Fibre-Reinforced Concrete, UHPFRC 2017.

22. H. Neuber (1969) "Der zugbeanspruchte Flachstab mit optimalem Querschnittsübergang," Forschung Im Ingenieurwesen, 35, pp. 29–30 (*in German*).
23. S.D.P. Benson and B.L. Karihaloo (2005) "CARDIFRC®-Development and mechanical properties. Part III: Uniaxial tensile response and other mechanical properties," Magazine of Concrete Research, 57, pp. 433–443.
24. Technical Leaflet SIA 2052 UHPFRC – Materials, design and construction, March 2016 (*in German and French*).
25. K. Habel; M. Viviani; E. Denarié; and E. Brühwiler (2006) "Development of the mechanical properties of an Ultra-High Performance Fiber Reinforced Concrete (UHPFRC)," Cement and Concrete Research, 36, pp. 1362–1370.